

PROCESSING AND CHARACTERISATION OF TANDEM SOLAR CELLS FROM CRYSTALLINE SILICON MATERIALS

S. Janz¹, M. Schnabel¹, P. Löper¹, C. Summonte², M. Canino²,
J. López-Vidrier³, S. Hernández³, B. Garrido³, S.W. Glunz¹

¹Fraunhofer Institut für Solare Energiesysteme, ²Consiglio Nazionale delle Ricerche – Istituto per la Microelettronica e i Microsistemi Bologna, ³Universitat de Barcelona – Departament d'Electrònica

Corresponding author: Stefan Janz, Fraunhofer Institut für Solare Energiesysteme, Heidenhofstrasse 2, D-79110 Freiburg, Germany, Ph +49 761 4588 5261, Fax +49 761 4588 9250.

ABSTRACT: We present the first crystalline Si-based tandem solar cell device consisting of a monolithically interconnected c-Si wafer bottom and a Si nanocrystal (NC) top solar cell. The major part of this work has been realised within a European consortium in the frame of the FP7 project NASCEnT. Within this project we have been able to (i) develop new nanomaterials with photovoltaic compatible technologies, to (ii) improve the theoretical understanding of transport, recombination and dopant incorporation in these quantum confined absorber materials and to (iii) design devices which enable us to prove quantum confinement. In this publication we show that although solid phase crystallisation at 1100 °C for around 30 min is necessary to generate Si NCs of proper quality the wafer bottom cell as well as the c-SiC(n⁺) tunnel recombination junction layer can withstand such harsh conditions. Besides simulations to determine the influence of the high thermal budget on dopant profiles in wafer and c-SiC lifetime measurements on parallel processed wafers still show minority carrier lifetimes of 600 μs. The bifacial character of the tandem device enables us to clearly distinguish between bottom and top cell contributions. With a NC layer thickness of initially 3 nm V_{oc} values as high as 978 mV could be achieved at 1 sun illumination from the front-side. Under rear-side illumination the short circuit current J_{sc} is with 1.0 mA/cm² 4 times higher than under front side illumination due to the better absorption and carrier lifetime of the bottom cell but still limited by the series resistance of the intrinsic NC absorber material. However, at 510 mV the V_{oc} is much lower, indicating the difference in V_{oc} is due to photogenerated voltage in the NC top cell which can only be created by illumination with low-wavelength light, i.e. front illumination. This very first tandem solar cell device including quantum dot absorber layers produced with photovoltaic compatible processes is the next step to successfully overcome the Shockley-Queisser limit for wafer based Si solar cells.

Keywords: Quantum Dots, Nanoparticles, Devices, Tandem

1 INTRODUCTION

Crystalline silicon wafer solar cells have been dominating the photovoltaic (PV) market so far. Availability and stability of crystalline silicon and the decades of Si technology development together with the non-toxicity of the material are the main reasons for that success. Record efficiencies with up to 25 % [1] could be shown but their maximum efficiency is limited to 29.4 % [2] due to different loss mechanisms. Without strategies to circumvent this limitation the c-Si technology will not be able to maintain its dominant role in the PV market. However, thermalisation losses can be reduced by adding a top cell with a higher band gap above a conventional silicon cell to create a tandem cell with potentially more than 40 % efficiency [3]. Silicon quantum dots (Si QDs) are a promising candidate for the top cell of an all-Si tandem solar cell, with a band gap that is tuneable from 1.3-1.7 eV [4, 5] by adjusting QD size. They are readily produced within a Si-based dielectric matrix by precipitation from a stack of alternating Si-rich and stoichiometric dielectric layers [6]

In order to exploit the potential of band gap engineered silicon nanocrystals for photovoltaics we have been working within the NASCEnT project on all key issues like (i) enhanced material quality of silicon superlattices [7, 8] and doping [9, 10], (ii) theoretical simulation, and comparing Si QDs superlattices in SiC, SiN_x and SiN_xO_y matrices (Si/SiC, Si/SiN_x and Si/SiN_xO_y), (iii) advanced structural characterisation [11] and (iv) devices to prove quantum confinement [12] as well as the very first all-Si tandem solar cell. Important features of the device such as emitter, passivation layer

and tunnel junction for tandem cell integration have developed within this project. In this publication we will focus on processing and characterisation of the first tandem solar cell device which is the monolithical interconnection of a wafer based and a QD absorber cell with Si nanocrystals inside a SiC matrix.

2 METHODS

2.1 Tandem Solar Cell Device

The device structure produced within this work is shown schematically in Figure 1. The deep boron emitter was manufactured on a FZ-Si wafers (400 μm, 5 Ω cm, <100>) by a boron tribromide (BBr₃) diffusion followed by a drive-in step under Ar, with 500 nm SiO₂ deposited on the rear-side of the wafer by plasma enhanced chemical vapour deposition (PECVD) before diffusion to ensure a one-side diffusion only. The diffusion barrier performance of the PECVD SiO₂ was tested by 4-point probe sheet resistance measurements and found to be successful before diffusing the tandem cell wafers. Wafers received an RCA clean before the SiO₂ deposition, and were cleaned in hot nitric acid (HNO₃) and HF before the diffusion step. After diffusion and drive-in the PECVD SiO₂ was removed in the same HF etching step as the borosilicate glass (BSG).

Following the emitter diffusion 1 μm of SiC(n⁺) was deposited by atmospheric pressure (AP)CVD at 1100 °C from precursor gases Methyltrichlorosilane (MTS), H₂ and N₂. In the first batch, in which all the tandem cells with Si NC/SiC layers were produced, there was significant parasitic deposition of SiC(n⁺) on the rear side

of the wafers. This was subsequently removed by reactive ion etching using Ar, H₂ and SF₆. However, since the etch rate is much higher in Si than in SiC, and since the parasitic absorption was inhomogeneous, this led to distinct areas of the wafer having increased surface roughness. These local rough areas were to some extent eliminated by a TMAH etch performed later in the process chain, but never fully removed and remain present in the final devices. However, this does not appear to strongly compromise the devices, perhaps because there is no charge-separating junction on the rear-side of the device.

The wafers then received another RCA clean before deposition of the Si NC/SiC precursor layers by PECVD [13]. A thin a-Si:H film is deposited on top of the precursor layer to prevent the precursor from oxidising during annealing [14]. All wafers (except 2 reference samples) were then annealed at 600 °C for 4 h followed by 1100 °C for 30 min under N₂/10 % O₂ with heating and cooling ramps of 5 °C/min. In order to remove the thermal oxide formed during this anneal, as well as the sacrificial capping layer deposited on the Si NC/SiC precursor layers, the samples were then etched in HF, then TMAH, and then again in HF. Some samples were processed in a remote plasma hydrogen passivation (RPHP) system at 450 °C for 45 min in order to reduce dangling bonds and other defects.

The cell process was completed with standard heterojunction solar cell processing. Wafers were first cleaned in hot HNO₃ and HF, then 25 nm of a-Si_{0.95}C_{0.05}(n):H were deposited on the rear side by PECVD from precursor gases silane (SiH₄), methane (CH₄), H₂ and Ar. On the front side of the wafers 5 nm a-Si(i):H and 25 nm a-Si(p):H were deposited [12]. Finally, the wafers were dipped in 1 % HF and 70 nm ITO were sputtered on both front- and rear-side. Metal grids consisting of a thermally evaporated 50 nm Ti / 50 nm Pd / 2000 nm Ag stack which were implemented on front and rear side using photolithography and lift-off. The 2 x 2 cm² device area was defined by performing a mesa etch of the ITO on front- and rear-side using photolithography and etching in concentrated HCl.

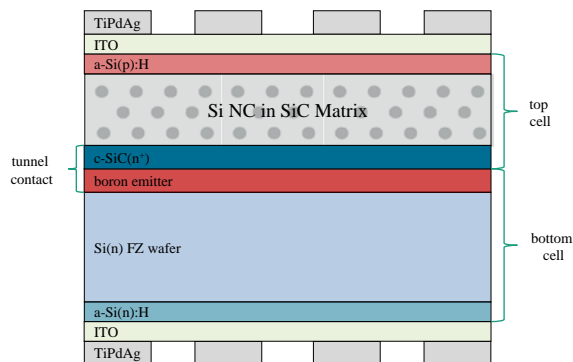


Figure 1: Structure of the tandem solar cell including the Si wafer bottom and the Si nanocrystal (NC) top solar cell interconnected by a c-Si(p⁺) / c-SiC(n⁺) contact (tunnel recombination junction).

The IV measurements, in dark and under illumination, were carried out with four-point probing using a Keithley source meter. For the electrical characterization under illumination, an Oriel solar simulator was employed as light source, simulating the AM1.5 spectrum. The irradiance was set to 1000 W/m²

using a calibrated c-Si solar cell as reference.

2.2 Influence of Thermal Budget on Si Wafer Bottom Solar Cell and Tunnel Junction

One of the most critical issues when developing a wafer bottom solar cell as well as a contact for monolithical interconnection to the top cell is the thermal budget of 1100 °C for 30 min which has to be applied to achieve good nanocrystal qualities in the top solar cell with solid phase crystallisation (SPC), given that the top cell is processed on top of the bottom cell. To test for lifetime degradation that would affect the Si wafer bottom cell lifetime samples were processed in parallel to the tandem cells, using the same wafers as used for the cells. Some were annealed at 1100 °C, some were not, and similarly from each group half were etched in hydrofluoric acid (HF), tetramethylammonium hydroxide (TMAH) plus HF and half were etched in HF only to see whether the TMAH etch causes surface roughness that compromises surface passivation. Passivation was carried out by depositing the same a-Si(n):H layer used as the bottom cell back surface field (BSF) in the tandem cell. The boron emitter was designed to withstand the same thermal budget without spreading out excessively, and in particular, without the boron concentration at the SiC(n⁺) / Si(p⁺) interface decreasing so much as to impede transport across this tunnel recombination junction. In order to aid in this we performed simulations of diffusion at this junction for a deep boron emitter manufactured (see section 2.1). Diffusion constants ranging from 1.5x10⁻¹¹ cm²s⁻¹ to 1.5x10⁻¹³ cm²s⁻¹ (1.5x10⁻¹¹ cm²s⁻¹ being the highest reported value for comparable material in the literature [15]) were assumed for boron diffusion in the SiC at 1100 °C, as well as a segregation coefficient of 20 favouring the SiC [16]. Furthermore, we measured by means of electrochemical capacitance voltage (ECV) the resulting dopant profiles in reference wafers.

3 RESULTS

3.1 Si Wafer Bottom Solar Cell

High-temperature annealing is known to affect the minority carrier lifetime in FZ-Si wafers [17]. In order to determine the role of this effect in our work we processed lifetime samples described in Section 2.2 and measured lifetimes by QSSPC in transient mode. We find that annealing at 1100 °C for 30 min causes a decrease in minority carrier lifetime by an order of magnitude, from 8000 μs to 600 μs (see Figure 2). However, the latter still corresponds to a minority carrier diffusion length of about 850 μm, sufficient to extract most carriers from a 400 μm wafer. The TMAH etch improves carrier lifetime. This means its roughening of the wafer surface has a negligible effect on surface passivation quality. The reason for the increase may lie in the limitation of the lifetime of annealed wafers being due to in-diffusion of impurities at the surface, which are removed by TMAH, but a detailed understanding of this phenomenon is outside the scope of this investigation and has no effect on the tandem solar cell process.

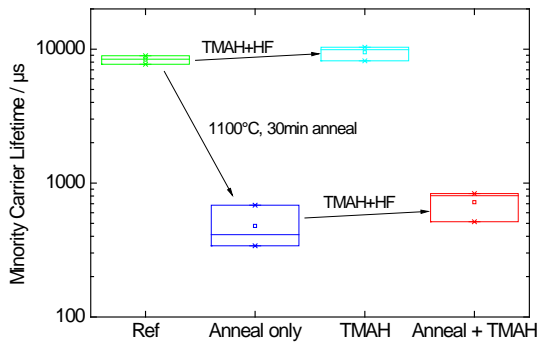


Figure 2: Minority carrier lifetimes determined by quasi-steady state photo conductance (QSS-PC) decay measurement on 400 μm , 5 Ωcm FZ-Si wafers as a function of annealing and/or wet chemical treatment.

Having checked the lifetime in the base, it was then necessary to investigate the change of the emitter due to the high-temperature annealing. The ECV measurements in Figure 3 show that the emitter profile can withstand the thermal budget for c-SiC deposition and NC formation without breakdown of the p-n junction of the bottom cell. The emitter is rather deep, but since the blue response of the tandem cell is determined by the top cell anyway this seems to be no major drawback for the whole device. However, the high dose of boron is necessary for reasons discussed in the next section.

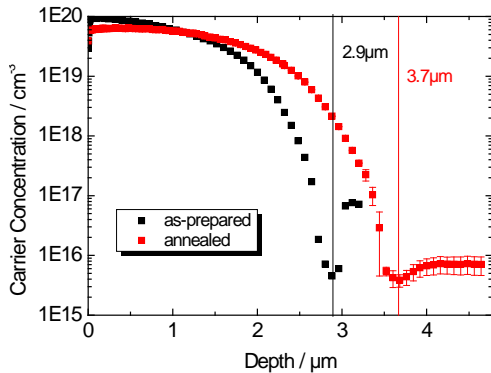


Figure 3: Electrochemical capacitance voltage (ECV) measurements of the boron profiles measured before and after processing of the tandem cells on reference samples. The junction depths are labelled in the figure.

3.2 Contact for Monolithic Interconnection

The influence of diffusion on the tunnel junction connecting top and bottom cell due to the thermal budget could not be carried out by ECV because c-SiC is not etched by common etchants. Simulations were therefore carried out to determine the effect of the thermal budget on carrier concentrations at this junction (see Figure 4). The diffusivity in the polycrystalline SiC was varied between $1.5 \times 10^{-13} \text{ cm}^2 \text{ s}^{-1}$ (blue) and $1.5 \times 10^{-11} \text{ cm}^2 \text{ s}^{-1}$ (green). This makes a big difference to the interface concentration which is $1 \times 10^{19} \text{ cm}^{-3}$ or a few $1 \times 10^{18} \text{ cm}^{-3}$, respectively. The effect of varying the segregation coefficient between 15 (solid line) and 20 (dotted line) for both cases is also shown. Having an interface boron concentration of only a few $1 \times 10^{18} \text{ cm}^{-3}$ is too low for degenerate doping, which is needed for true tunnel junctions. However, test devices with such boron concentrations have still resulted in SiC(n⁺)/Si(p⁺) junctions with ohmic behaviour. This means that the

selected boron profile is suitable for the application in first tandem solar cell devices. However, reduction of thermal budget for SPC and initially higher dopant levels in both materials leading to more shallow junctions will be one major task to improve this tandem device structure.

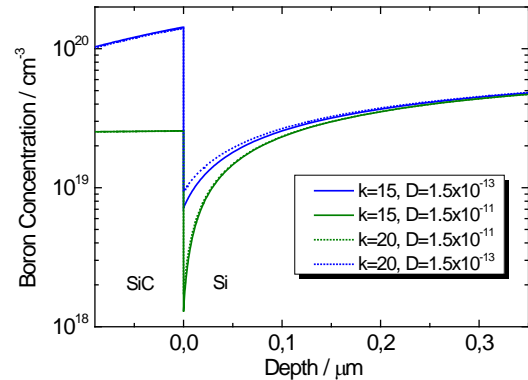


Figure 4: Simulation of boron diffusion in c-Si bulk (right), c-SiC contact layer (left) with diffusivities in SiC of $1.5 \times 10^{-13} \text{ cm}^2 \text{ s}^{-1}$ (blue) and $1.5 \times 10^{-11} \text{ cm}^2 \text{ s}^{-1}$ (green) and different segregation coefficients of 15 (solid) and 20 (dotted).

3.3 Tandem Solar Cell Devices

The tandem solar cells were measured under dark conditions first to see if a fit to the 2 diode model is possible (see Figure 5). With $n_1=1.00$ and $n_2=2.00$ we could extract a $J_{01}=1.00 \times 10^{-7} \text{ A/cm}^2$ and a $J_{02}=1.06 \times 10^{-5} \text{ A/cm}^2$ as well as series and parallel resistance values of $R_s=35.0 \Omega \text{ cm}^2$ and $R_p=30.5 \Omega \text{ cm}^2$ for the one sample with a nominal Si rich carbide (SRC) layer thickness of 5 nm (solar cell area of 4 cm^2).

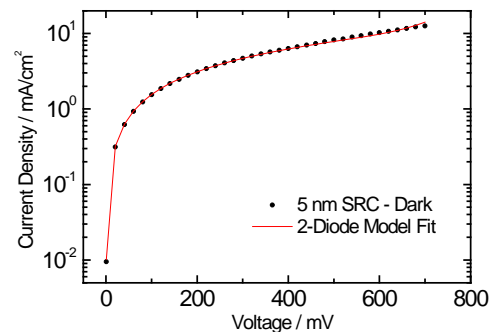


Figure 5: IV characteristic in dark for the cell containing Si rich carbide (SRC) layers with an initial thickness of 5 nm as top-cell absorber material.

In Figure 6 the effect of the initial SRC layer thickness (i.e. the nominal Si NC size) on the tandem cell performance is shown. It seems that the thinnest SRC layers show the highest V_{oc} . A possible explanation could be the greater absorption efficiency of high-energy photons presented by the smaller NCs. Moreover, if we consider that the current from the top cell may be transport-limited, the thinner this layer the higher the carrier extraction capability of the tandem cell should be. What is clear is the fact that almost all measured devices (>30) show the same curve shape under front-side illumination and present very similar efficiency values (0.3 – 0.5 %), with fill factors ranging between 0.2 and 0.4. Although this is the first time that such quantum dot

structures have been implemented into a monolithically interconnected tandem solar cell device on a c-Si wafer this statistic proves the reliability of our newly developed process sequence.

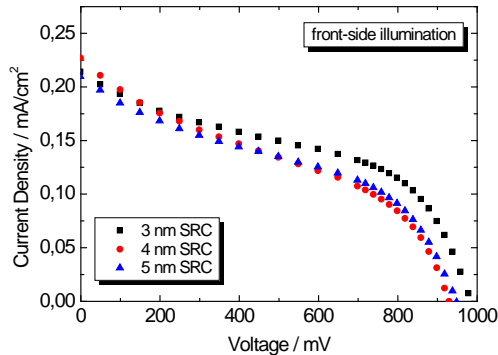


Figure 6: IV characteristic under illumination from the front-side for SRC layers with 3, 4 and 5 nm initial thickness.

One additional advantage of our device is its bifacial character which enables direct comparison between front-side and rear-side illumination of the cell device. When illuminating from the front-side V_{oc} almost doubles its value compared to rear-side illumination (Figure 7). The most plausible explanation is the fact that the Si substrate (bottom cell) absorbs the short wavelength radiation of the spectrum when illuminating from the back. Thus no high-energy photons are available that could generate a photovoltage in the high bandgap NC top cell. As a result, a similar V_{oc} than the one expected from a single Si cell is obtained here. However, the IV characteristic shows a very low fill factor, which is due to the fact that the entire top cell is effectively not illuminated and acts as a high series resistance (see also Figure 5 which is fit with $R_s=35.0 \Omega \text{ cm}^2$).

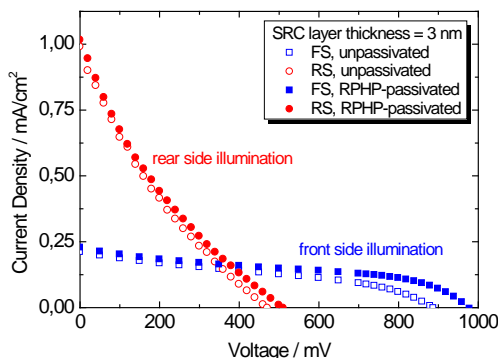


Figure 7: IV characteristic under illumination from front (blue) - as well as from rear-side (red) for SRC layers with 3 nm initial thickness. For some solar cells remote hydrogen passivation (solid symbols) was done.

On the other hand, when illuminating the front-side the tandem cell acts as desired: high-energy photons are absorbed by the top NC cell and the low-energy ones by the bottom c-Si cell. In other words, a series connection is established between both cells and leads to V_{oc} values of around 900 mV. The short-circuit current is limited by the less efficient top cell of the tandem stack (0.25 instead of 1 mA/cm²). In Figure 8 the positive effect of remote plasma hydrogen passivation (RPHP) on the solar cell performance is shown in detail. The passivation of

dangling bonds especially at the Si NC interface to the matrix can explain the significant improvement of V_{oc} up to almost 1 V. Even the bottom solar cell seems to benefit from the hydrogen passivation layer, perhaps because passivation of defects in the Si NC layer reduces the series resistance it creates. The slightly higher values for J_{sc} after passivation may be attributed to a better electrical performance of the NC layer.

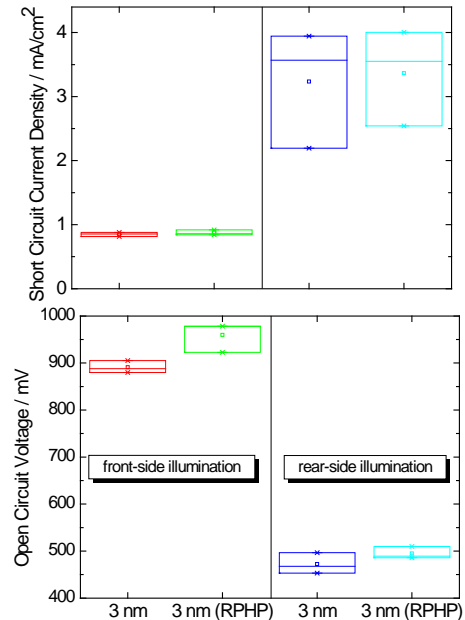


Figure 8: Short circuit current densities and open circuit voltages under front-side and rear-side illumination for samples (SRC layers with 3 nm nominal thickness) with and without remote plasma hydrogen passivation.

4 CONCLUSIONS

After three years of project duration the European NASCEnt consortium was successful in realising the first all-crystalline-Si tandem solar cell device including quantum dot absorber layers. The monolithically interconnected c-Si wafer bottom cell with a Si nanocrystal (NC) top solar cell device includes all features which are necessary to form a highly efficient solar cell device. We could prove that the Si wafer bottom solar cell as well as the c-SiC(n+) tunnel recombination junction are still functional despite having to endure a thermal budget of 1100 °C for 30 min. Illumination from front- or rear-side lead to V_{oc} s of >978 mV and 500 mV, respectively. This clearly proves the successful interconnection of the two solar cells. The J_{sc} measured with rear-side illumination is limited due to high series resistance of the intrinsic NC layer. A comparison of tandem cells with NC layers of different initial layer thicknesses shows no clear trend. However, the layer with the highest proposed bandgap leads to the record V_{oc} of 978 mV after hydrogen passivation. In order to improve the device efficiency NC material improvement is paramount. Besides that a low thermal budget route could further improve the performance of the Si-wafer bottom cell as well as the tunnel contact. The very first and functional tandem solar cell device including quantum dot absorber layers is the next step to

successfully overcome the Shockley-Queisser limit for wafer-based Si solar cells.

5 ACKNOWLEDGEMENTS

The authors would like to thank their colleagues for valuable advice and discussions. We especially thank A. Leimenstoll, F. Schätzle, S. Seitz and Nadine Weber for processing, K. Schillinger for the development of the SiC (n^+) layer and J. Schön for the diffusion simulations. The research leading to these results has received funding from the European Community's Seventh Framework Programme (FP7/2007-2013) under grant agreement n°: 245977 under the project title NASCEnt. P. Löper gratefully acknowledges the scholarship support from the Reiner Lemoine Stiftung, and the ideational support from the Heinrich Böll Stiftung.

6 REFERENCES

- [1] Green, M.A., *et al.*, Prog. Photovolt: Res. Appl. 2013; 21:827–837
- [2] A. Richter, A., *et al.*, IEEE Journal of Photovoltaics, Vol 3(4), p.1184 – 1191.
- [3] Green, M.A., Springer Series in Photonics, ed. T. Kamiya, *et al.*, Vol. 12. 2003, Berlin, Heidelberg, New York: Springer. 160.
- [4] Conibeer, G., *et al.*, Thin Solid Films, 2006, 511-2: p. 654-62.
- [5] Löper, P., *et al.*, Proceedings of the 24th European Photovoltaic Solar Energy Conference, 2009, Hamburg (Germany) p. 734-738.
- [6] Zacharias, M., *et al.*, Applied Physics Letters, 2002, 80(4): p. 661-3.
- [7] Hartel A.M., *et al.*, Thin Solid Films 520 (2011) 121-125.
- [8] Hiller, D., *et al.*, Journal of Applied Physics 109 (2011) 054308.
- [9] Gutsch, S., *et al.*, Applied Physics Letters 100 (2012) 233115.
- [10] Summonte, C., *et al.*, Materials Science & Engineering B 178(9) (2013) 551-558.
- [11] López-Vidrier, J., *et al.*, Materials Science & Engineering B 178(9) (2013) 639-644.
- [12] Löper, P., *et al.*, Advanced Materials 24 (2012) 3124-3129.
- [13] Schnabel, M., *et al.*, Solid State Phenomena Vols. 205-206 (2014) pp 480-485.
- [14] Canino, M., *et al.*, Materials Science & Engineering B 178(9) (2013) 623-629.
- [15] Atabaev, G.I., *et al.*, Materials Sciences and Applications, 2011, 2, 1205-1211.
- [16] Janz, S., PhD thesis, Dr. Hut Verlag, ISBN:978-3-89963-563-8, p.125.
- [17] Poggi, A., *et al.*, J. Electrochem. Soc., Vol. 141, No.3 (1994) pp. 754-758.